Molecular Biology of the Cell
Vol. 15, 4710–4724, October 2004

Golgi Enzymes Are Enriched in Perforated Zones of Golgi Cisternae but Are Depleted in COPI Vesicles

Hee-Seok Kweon,*† Galina V. Beznoussenko,*† Massimo Micaroni,* Roman S. Polishchuk,* Alvar Trucco,* Oliviano Martella,* Daniele Di Giandomenico,* Pierfrancesco Marra,* Aurora Fusella,* Alessio Di Pentima,* Eric G. Berger,*‡ Willie J. C. Geerts,*§ Abraham J. Koster,*§ Koert N. J. Burger,*§ Alberto Luini,*‖ and Alexander A. Mironov*‖¶

*Department of Cell Biology and Oncology, Consorzio Mario Negri Sud, 66030 Santa Maria Imbaro (Chieti), Italy; ‡Institute of Physiology, University of Zurich, CH-8057 Zurich, Switzerland; and §Department of Molecular Cell Biology, Institute of Biomembranes, Utrecht University, 3584 CH Utrecht, The Netherlands

Submitted December 11, 2003; Accepted June 29, 2004
Monitoring Editor: Keith Mostov

In the most widely accepted version of the cisternal maturation/progression model of intra-Golgi transport, the polarity of the Golgi complex is maintained by retrograde transport of Golgi enzymes in COPI-coated vesicles. By analyzing enzyme localization in relation to the three-dimensional ultrastructure of the Golgi complex, we now observe that Golgi enzymes are depleted in COPI-coated buds and 50- to 60-nm COPI-dependent vesicles in a variety of different cell types. Instead, we find that Golgi enzymes are concentrated in the perforated zones of cisternal rims both in vivo and in a cell-free system. This lateral segregation of Golgi enzymes is detectable in some stacks during steady-state transport, but it was significantly prominent after blocking endoplasmic reticulum-to-Golgi transport. Delivery of transport carriers to the Golgi after the release of a transport block leads to a diminution in Golgi enzyme concentrations in perforated zones of cisternae. The exclusion of Golgi enzymes from COPI vesicles and their transport-dependent accumulation in perforated zones argues against the current vesicle-mediated version of the cisternal maturation/progression model.

INTRODUCTION

The mechanisms of secretory transport through the Golgi remain an issue of debate. Several transport schemes are under consideration in the search for a new paradigm in the field of intracellular secretory transport (reviewed in Griffiths, 2000; Beznoussenko and Mironov, 2002; Elsner *et al*., 2003). With the old vesicular model not able to explain the exclusion of most cargoes from COPI-dependent vesicles (Bonfanti *et al*., 1998; Beznoussenko and Mironov, 2002; Elsner *et al*., 2003), the most favored model is now the cisterna maturation model. Here, material exiting from the endoplasmic reticulum (ER) converges toward the Golgi complex and forms a new *cis*-cisterna. The nonsecretory material (e.g., ER-resident proteins) is retrieved from the *cis*-Golgi into the ER, whereas at the same time the defining components of the medial compartment (e.g., medial Golgi enzymes) flow "backwards" into the *cis*-elements. The *cis*-compartment thus acquires medial Golgi features, and in effect becomes a medial compartment. This process repeats itself (the medial compartment becoming *trans*) until the cargo reaches the *trans*-Golgi network (TGN). Finally, the secretory material in the TGN is progressively released through the formation of secretory granules and/or vesicles, or via other mechanisms that consume the organelle. TGN-resident proteins then recycle back to the *trans*-Golgi, thereby transforming it into the next TGN ready for secretion. The essential characteristic of this mechanism is the maturation of the cisternae, with the consequence that cargo progresses through the stack. The main feature of the model is that Golgi enzymes concentrate in COPI-dependent vesicles, within which they then move backwards through the stack in synchrony with the progression of the cisternae.

Testing the current version of the cisternal maturation/progression model of intra-Golgi transport has given conflicting results. Indeed, some authors have shown that coated (presumably by COPI) peri-Golgi round profiles, which were assumed to represent vesicles, contain the Golgi enzyme mannosidase (Man)II in vivo at concentrations similar to or higher than those in cisternae (Martinez-Menarguez *et al*., 2001). Others, however, have reported the depletion of ManII in peri-Golgi round profiles (Orci *et al*., 2000), and recently Cosson *et al*. (2002) showed a 3.2- to 4.9-fold level of ManII exclusion from peri-Golgi round profiles under essentially the same conditions as those used by Martinez-Menarguez *et al*. (2001). Finally, in in vitro studies, small membrane fragments (again assumed to represent bona fide COPI vesicles) enriched in Golgi enzymes and

Article published online ahead of print. Mol. Biol. Cell 10.1091/mbc.E03–12–0881. Article and publication date are available at www.molbiolcell.org/cgi/doi/10.1091/mbc.E03–12–0881.

† These authors contributed equally to this work.

‖ Principal investigators.

¶ Corresponding author. E-mail address: mironov@negrisud.it.

Abbreviations used: 3D, three-dimensional; Ab, antibody; COP, coat protein; FP, fluorescent protein; GalT, galactosyltransferase; LD, labeling density; Man, mannosidase; PC, procollagen I; STF, sialyltransferase; VSVG, temperature-sensitive variant of the G protein of vesicular stomatitis virus.

dependent on COPI and GTP hydrolysis by ARF1 for their formation, have been isolated after incubation of isolated Golgi membranes with cytosol and GTP (Lanoix *et al*., 1999, 2001).

In the current study, we have used several independent approaches that were designed to resolve these controversies. By combining enzyme localization with a three-dimensional (3D) analysis of Golgi ultrastructure and the biochemical isolation of COPI-dependent vesicles, we find that COPI-dependent vesicles are depleted of Golgi enzymes and are thus unlikely to be the retrograde carriers of Golgi enzymes.

MATERIALS AND METHODS

Human fibroblasts were from Dr. M. DeLuca (Istituto Dermatopatico dell'Immacolata, Rome, Italy), normal rat kidney (NRK) cells stably transfected with sialyltransferase (STF)-horseradish peroxidase (HRP) were from Dr. E. Jokitalo (University of Helsinki, Helsinki, Finland), ssHRP-KDEL cDNA was from Dr. D. F. Cutler (University College London, London, United Kingdom), the His6-α-SNAP and His6-α-SNAP (L294A) mutant cDNAs were from Dr. R. Burgoyne (University of Liverpool, Liverpool, United Kingdom), the ManI and ManII cDNAs and the ManI and ManII polyclonal antibodies were from Dr. K. W. Moremen (University of Georgia, Athens, GA), the antibody against the COOH-terminal peptide of the α-1 chain of procollagen I (PC) was from Dr. L. W. Fisher (National Institutes of Health, Bethesda, MD), the temperature-sensitive variant of the G protein of vesicular stomatitis virus (VSVG) luminal domain monoclonal antibody was from Dr. J. Gruenberg (University of Geneva, Geneva, Switzerland), the VSVG luminal domain polyclonal antibody and ts045-VSV were from Dr. K. Simons (Max-Planck-Institute, Dresden, Germany), and protein A conjugated with colloidal gold was from Dr. J. Slot (Utrecht University, Utrecht, The Netherlands). Unless otherwise stated, all other chemicals and reagents were obtained from previously indicated sources (Mironov *et al*., 2001) or from Sigma (Milan, Italy).

To prepare the ManI-YFP and ManII-YFP constructs, the *Eco*RI and *Sac*II restriction sites were added by polymerase chain reaction (PCR) at 5′ and 3′, respectively, of the ManI gene by using as primers the following oligonucleotides: 5′-GCGGAATTCATGCCCGTGGGGGGCCTGT-3′ and 5′-GCGCCGCGGTTTCTCTTTGCCATCAATT-3′. The *Bam*HI and *Eco*RI restriction sites were added by PCR at 5′ and 3′, respectively, of the ManII gene by using as primers the following oligonucleotides: 5′-GCGGATCCATGAAGTTAAGTCGCCAGT-3′ and 5′-GCGGAATTCGGGTCCAACGCAAGCGGATA-3′. The amplification product was subcloned into a *Bam*HI/*Eco*RI-digested pEYFPN1 (BD Biosciences Clontech, Palo Alto, CA) plasmid. The synchronization of cargo movement along the secretory pathway was performed as described previously (Mironov *et al*., 2001). Two types of cargo synchronization protocols were used. Briefly, human fibroblasts infected with vesicular stomatitis virus (VSV) were incubated for 3 h at the restrictive (40°C) temperature (to block VSVG exit from the ER) in the absence of ascorbic acid (to block PC exit from the ER). Next, VSVG and PC were accumulated in the intermediate compartment by placing the cells at 15°C for 15 min (the miniwave protocol) or 2 h (the maxiwave protocol) (Mironov *et al*., 2001). Finally, the 15°C temperature block was released, the temperature (40°C)/hydroxylation (absence of ascorbic acid) blocks were reinstalled, and the passage of cargo through the Golgi was monitored. Cells were fixed 0, 7, 12, and 18 min after the shift to 40°C and the elimination of ascorbic acid from the medium, and prepared for electron microscopy (EM).

Golgi membranes were incubated in a K^+-rich transport buffer with cytosol, GTP, and an ATP regeneration system, and without or with addition of the His6-α-SNAP mutant, as described by Lanoix *et al*. (1999), with minor modifications, which included a higher concentration (7 mg/ml) of cytosol and a longer incubation (90 min). Coatomer-depleted cytosols, purified coatomer, and recombinant ARF1 were prepared exactly as described previously (Godi *et al*., 1998). The His6-α-SNAP (L294A) mutant was prepared as described previously (Barnard *et al*., 1996). Culturing of human fibroblasts, and COS7, NRK and rat basophilic leukemia (RBL) cells, infection with ts045-VSV, transfection of cells by electroporation (to avoid transfection artifacts, only cells with a minimal visible level of expression of the constructs were examined, 16 h after transfection), stimulation of PC synthesis in human fibroblasts, fluorescence microscopy analysis, conventional and immuno-EM, 3D reconstructions of EM serial sections, correlative light-EM, ultrathin cryosectioning, rapid freezing-cryosubstitution, and analysis of samples by EM tomography were all carried out as described previously (Mironov *et al*., 2001). Brief descriptions are given below.

Electron Microscopy

Cells were plated in eight-well glass chamber slides (NUNC A/S, Roskilde, Denmark) and used for experiments after 24 h at 90% confluence. They were then fixed with 1% glutaraldehyde in 0.15 M HEPES (pH 7.3) at 37°C for 5 min and kept in the same solution for 60 min at room temperature. After this fixation, the cells were treated with 1% OsO_4 plus 1.5% potassium ferrocyanide in 0.1 M cacodylate buffer (pH 7.3) for 2 h on ice (all incubations before this step were performed at room temperature) in the dark and embedded in Epon 812. For immuno-EM, the cells were fixed with 4% formaldehyde and 0.05% glutaraldehyde for 10 min at 37°C and then postfixed for 50 min with 4% formaldehyde alone, at room temperature. After washing and a 20-min treatment with a blocking solution containing 1% bovine serum albumin, 50 mM NH_4Cl, and 0.2% saponin, the samples were incubated with the necessary antibodies for 2 h. Primary antibodies were detected with monovalent Fab fragments of goat anti-rabbit IgG conjugated with HRP (Biosys, Compiegne, France) and subsequent diaminobenzidine (DAB) developed as described previously (Brown and Farquhar, 1989). Then, the cells were postfixed with reduced OsO_4, and embedded in Epon 812.

Correlative Light Electron Microscopy

COS7 cells were grown on CELLocate coverslips (MatTek Corporation, Ashland, MA) in DMEM supplemented with 10% fetal calf serum and 2 mM glutamine. The cells were initially fixed and prepared as for immuno-EM (see above). Then, before embedding, the samples were analyzed under the laser-scanning electron microscope (LSCM), and the cell of interest underwent optical sectioning along the z-axis when its position within the coordinated grid had been determined. Next, the samples were incubated for 60 min with nanogold-conjugated Fab fragments of an anti-rabbit IgG (NanoProbes, Yaphank, NY) diluted in blocking solution (1:100) and then extensively washed and fixed with 1% glutaraldehyde in 0.2 M HEPES (pH 7.3) for 5 min. Gold particles were enhanced by GoldEnhancer (NanoProbes) according to the manufacturer's instructions. Routinely, the time of enhancement was ~4–6 min. After osmium treatment (see above), the samples were embedded in Epoxy resin and polymerized for at least 24 h. The CELLocate coverslips were then dissolved with 40% hydrofluoric acid, and the samples were intensively washed with buffer and then distilled water. Finally, the cell of interest was sectioned tangentially. Sixty-nanometer serial sections were collected on slot grids covered with Formvar-carbon supporting film and examined at 80 kV in a Zeiss 109 electron microscope. The images collected by LSCM and EM were aligned with Adobe Photoshop, and the structure of interest was identified on the basis of its position in space and its labeling with colloidal gold. Cryoimmuno-EM labeling was performed according to Martinez-Menarguez *et al*. (2001) and Cosson *et al*. (2002).

Serial Sectioning, 3D Reconstruction, and Electron Tomography

Thin serial sectioning and 3D reconstructions were performed as described previously (Mironov *et al*., 2001). The analysis of samples by electron tomography was performed as described previously (Ladinsky *et al*., 1999; Mironov *et al*., 2001, 2003). Briefly, thick (200-nm) sections of chemically fixed samples were covered with 10-nm colloidal gold. Next, automated data acquisition was carried out, as described previously (Mironov *et al*., 2001), on a Tecnai 12 or 20 electron microscope at 120 or 200 kV (FEI/Philips Electron Optics, Eindhoven, The Netherlands) equipped with a slow-scan charge-coupled device camera (TemCam F-214, TVIPS, Germany) and a motorized goniometer. Finally, after alignment of the data stack by using the colloidal gold as marker and reconstruction with the IMOD program package (University of Denver, Denver, CO), 2- to 3-nm virtual slices were extracted from the tomograms and visualized. Object surfaces were rendered using the SURFdriver and IMOD softwares.

Morphometry

The counting of labeling densities (LDs) and the subtraction of the backgrounds (LDs over mitochondria) were performed as described previously (Mayhew *et al*., 2003), with minimal modifications. Briefly, we initially estimated the number of gold particles per micrometer of membrane length; then, round profile LDs were normalized with respect to cisternae LD as 100%. Round profiles were defined according to Misteli and Warren (1995) as being localized inside the Golgi zone of exclusion. We analyzed 50- to 60-nm round profiles because the actual Golgi vesicles have an average diameter of 52 nm (Marsh *et al*., 2001). All 50- to 60-nm round profiles found in the Golgi area, i.e., inside the zone of exclusion, were defined as peri-Golgi round profiles, whereas round profiles located within 40 nm of the rim of a cisterna were defined as near-rimmal round profiles. Nonrimmal round profiles are thus represented by peri-Golgi round profiles minus near-rimmal round profiles. Elongated profiles (with a length to width ratio >1.5) also include a small fraction of round profiles >65 nm. In tangential thin sections, the absence of a translucent lumen served as the criterion for the classification of 50- to 60-nm peri-Golgi round profiles as vesicles (Morre and Keenan, 1994). In thick sections, vesicles were defined as those round profiles that remained round during tilting of a section (+60 to −60°).

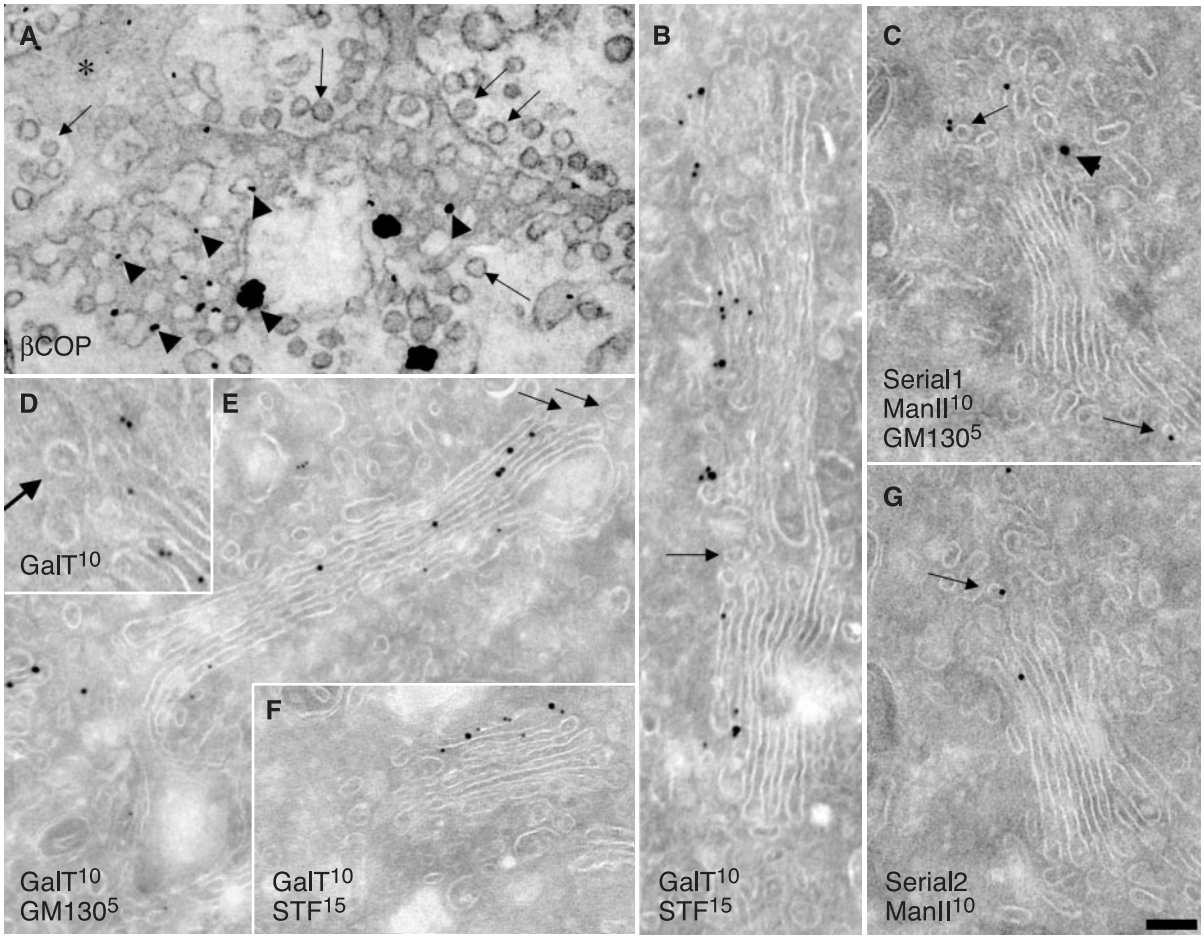

Figure 1. Composition of Golgi vesicles and tubules at steady state. NRK (A) and RBL (C and G) cells and human fibroblasts (B and D–F) were prepared for immuno-nanogold (A) or cryogold (B–G) EM. β-COPI was labeled with nanogold (A); GalT with 10-nm gold (B and D–F); GM130 with 5-nm gold (E) or with 15-nm gold (C, arrowhead); ManII with 10-nm gold (C and G); and STF with 15-nm gold (B and F). (C and G) Serial cryosections. (A) β-COPI (arrowheads) is present on perforated zones of Golgi cisternae but not in vesicles (arrows); asterisk indicates solid part of a cisterna. Golgi enzymes are excluded from peri-Golgi round profiles (B, arrows) and COPI-coated buds (D, arrow). ManII is present in round profiles of noncompact zones (C and G, arrows). Bars, 100 nm (A and B); 120 nm (C and E–G); and 85 nm (D).

RESULTS

Golgi Enzymes Are Excluded from 50- to 60-nm Peri-Golgi Round Profiles

Because previous studies (Martinez-Menarguez *et al*., 2001; Cosson *et al*., 2002) have been based on measurements of LDs of ManII in cryosections (see *Materials and Methods*), we first used this technique to determine whether ManII and other Golgi enzymes are indeed present in peri-Golgi round profiles. These peri-Golgi round profiles were defined (see *Materials and Methods*) as roughly circular profiles localized inside the Golgi area within the zone of exclusion, and with a mean diameter of 52 nm (Marsh *et al*., 2001). Of particular note, although round profiles are generally considered to represent Golgi vesicles on cryosections, they also can result from cross sections of tubules or perforated rims, which are present in all cisternae (Ladinsky *et al*., 1999). To test this possibility, we analyzed tangential sections of Golgi stacks in NRK cells after labeling with a polyclonal anti-β-COP antibody (Ab; Pepperkok *et al*., 1993), with the preembedding nanogold technique followed by gold enhancement (see *Materials and Methods*). As shown in Figure 1A, in tangential sections of *cis*-Golgi cisternae, the majority of gold particles marking the presence of β-COP (arrowheads) are situated over perforated zones of the cisternae. Almost no labeling of 50- to 60-nm vesicles (arrows; see definition in *Materials and Methods*) and the solid parts of cisternae (asterisk) is seen. Thus, the presence of a COPI-like coat is not a unique characteristic of COPI vesicles or buds.

Next, using cryosections, we assessed the distribution of endogenous galactosyltransferase (GalT) and STF in human fibroblasts, ManII in NRK and RBL cells, and ManI and ManII (full-length proteins) tagged with yellow fluorescent protein (FP; these fusion proteins localize and behave as the native proteins do; unpublished data) in COS7 cells transiently transfected with these constructs at steady state (i.e., without previous synchronization of cargo movement). Figure 1, B–G, shows that in these cells at steady state, GalT, ManI-FP, ManII, and STF were labeled in Golgi cisternae with the expected distribution along the *cis–trans* axis (Rabouille *et al*., 1995). In contrast, when we specifically examined the peri-Golgi 50- to 60-nm round profiles, we found that they were depleted of these enzymes. The LD of gold particles over buds with a visible COP-like coat (where the upper surface of the section passed through the center of the bud; Figure 1D) was lower than that over cisternae. In particular, we examined 20 randomly selected round and

Table 1. Relative LDs of Golgi enzymes at steady state (cryosections)

GE, cell type (n)				LD [% cisternae (±SE)]					Ratio of $LD_{Cisternae}/LD_{Peri\text{-}Golgi\ RPs}$
				Cisternae	All peri-Golgi RPs	Near-rimmal RPs	Non-rimmal RPs	Elongated profiles	
ManII	NRK	(30)		100.0 (±24.8)	17.1 (±10.5)[a]	12.4 (±9.5)[a]	21.0 (±12.4)[a]	160.0 (±29.5)[a]	5.8
ManII-FP	COS7	(30)		100.0 (±25.0)	88.5 (±23.1)[b]	160.6 (±29.8)[a]	27.9 (±13.5)[a]	243.3 (±35.6)[a]	1.1
ManI-FP	COS7	(49)		100.0 (±15.4)	18.1 (±7.4)[a]	42.3 (±10.7)[a]	7.4 (±4.7)[a]	106.7 (±16.1)[b]	5.5
STF	HFs	(31)		100.0 (±20.6)	25.5 (±11.3)[a]	35.5 (±12.8)[a]	14.2 (±8.5)[a]	192.2 (±26.2)[a]	3.9
GalT	HFs	(20)	3 passages	100.0 (±45.6)	23.5 (±23.8)[a]	82.4 (±41.2)[b]	11.8 (±17.6)[a]	nd	4.3
		(30)	20 passages	100.0 (±24.8)	25.7 (±13.9)[b]	32.7 (±14.9)[a]	20.8 (±11.9)[a]	223.8 (±34.7)[a]	3.9

GE, Golgi enzyme; HFs, human fibroblasts; n, number of Golgi sections; nd, not determined; RPs, round profiles. Each value represents the average of n independent measurements from at least three different experiments. LD was determined over all cisternae without their subdivision into cis, medial, and trans compartments and over all peri-Golgi round profiles without selection of defined areas. Values are expressed as means (± standard error). Data are normalized considering LD over cisternae as 100%.

[a] Significantly different ($p \leq 0.05$) from cisternae.

[b] Not significantly different ($p > 0.05$) from cisternae.

bud-like profiles with a visible COPI-like coat (Figure 1D) and could not find gold labeling for GalT over any of them. The quantification in Table 1 confirms that the concentrations of the enzymes in round profiles (total population) are several (4- to 6)-fold lower than those of the corresponding enzymes over Golgi cisternae. An exception was ManII-FP in transfected COS7 cells, which was typically enriched in medial and *trans*-Golgi cisternae (unpublished data). Additionally, the enzyme was enriched in round profiles (Figure 1, C and G, and Table 1), which, as indicated above, consisted of cross sections of vesicles and tubules mostly of the noncompact zones, the highly perforated zones connecting cisternae of different stacks (Ladinsky *et al*., 1999).

To confirm these data, we exploited immuno-HRP–based labeling combined with a preembedding protocol and serial sectioning. Figure 2 shows that most of the labeling for ManII (Figure 2, A–C) in RBL cells and GalT (Figure 2, D and E) in human fibroblasts was localized within one (GalT), two, or three (ManII) cisternae close to the *trans*-side of the Golgi stacks, in agreement with previous reports (Velasco *et al*., 1993; Rabouille *et al*., 1995). When labeling was seen in round profiles in the vicinity of ManII-positive (Figure 2, A–C, arrowhead) cisternal rims, serial sectioning demonstrated that these ManII-positive round profiles represented cross sections of the cylinder-like cisternal rims around pores located near the rims (near-rimmal) in perforated zones of the cisternae, rather than vesicles (see scheme in Figure 2G). Bud-like profiles also were depleted of ManII (Figure 2F, arrowhead). An analysis of GalT in human fibroblasts yielded identical results, with no labeling present in round profiles (Figure 2, D and E). Because antibody penetration might depend on the detergent used for membrane permeabilization, different detergents (0.1% Triton X100, Figure 2I; 0.2% Nonidet P-40; unpublished data) were used in addition to saponin, which was used in the aforementioned experiments. Despite the lower preservation of Golgi ultrastructure under these conditions, the exclusion of labeling for ManII from peri-Golgi round profiles was confirmed.

Given the above-mentioned information, an important issue at this point is what round profiles (as seen in sections) actually represent in three dimensions. Considering that most perforations of Golgi cisternae are located in the vicinity of the cisternal rims (Ladinsky *et al*., 1999), many peri-Golgi round profiles might represent cross sections of these perforated zones (see scheme in Figure 2H). Given the diameter of most perforations (~40 nm), we have defined the round profiles located within 40 nm of the cisternal rims in these cross sections as perforated zones. To verify the validity of this criterion, we analyzed 50-nm serial cryosections of Golgi stacks from NRK cells (Figure 2, J–M). Indeed, a substantial proportion (30%) of the round profiles located in the vicinity (within 40 nm) of the cisternal rims represented cross sections of tangential tubules and perforated zones of cisternae, rather than actual vesicles (Figure 2, J–M) (most of remaining 70% represented true vesicles and vertical tubules). This problem might thus affect all estimations of LDs of Golgi enzymes >50- to 60-nm vesicles based on cryogold immuno-EM labeling.

Next, to further test the enzyme depletion in actual 50- to 60-nm vesicles, we applied an approach that is independent of antibody access to epitopes localized in the lumen of Golgi vesicles. NRK cells stably transfected with HRP-tagged STF (Stinchcombe *et al*., 1995; Jokitalo *et al*., 2001) were fixed with 1% glutaraldehyde, subjected to the HRP reaction procedure, and prepared for tomography. Note that the HRP method used does not suffer from permeabilization and most fixation artifacts (Stinchcombe *et al*., 1995). As expected, STF-HRP was found in the *trans*-cisternae/TGN (Figure 3A). Figure 3, B–F, shows that whereas in single virtual sections some STF-positive round profiles were visible (Figure 3, D–F, arrows), these were cross sections of STF-positive tubules or perforated zones of cisternae (Figure 3, B and C). Similarly, no labeling of vesicles was seen in tangential sections of stacks (unpublished data). Moreover, there was no signal for STF in cisternal buds with a COPI-like coat (Figure 3, G–I, arrows). These buds are present not only on the *trans*-most cisterna but also on the medial one, indicating that these should not be clathrin coated, because clathrin-coated buds have been seen to be present exclusively on the *trans*-most cisterna of Golgi stacks (Ladinsky *et al*., 1999). As a positive control to be sure that this method can detect luminal molecules in vesicles, if present, we transiently transfected NRK cells with an $ssHRP^{KDEL}$ construct (Stinchcombe *et al*., 1995). The presence of the KDEL receptor in COPI vesicles has been documented in vivo (Orci *et al*., 1997) and in vitro (Yang *et al*., 2002). The cells were subjected to an identical procedure, and a clear signal was seen in bona fide 50- to 60-nm vesicles (Figure 3, J–L, arrows).

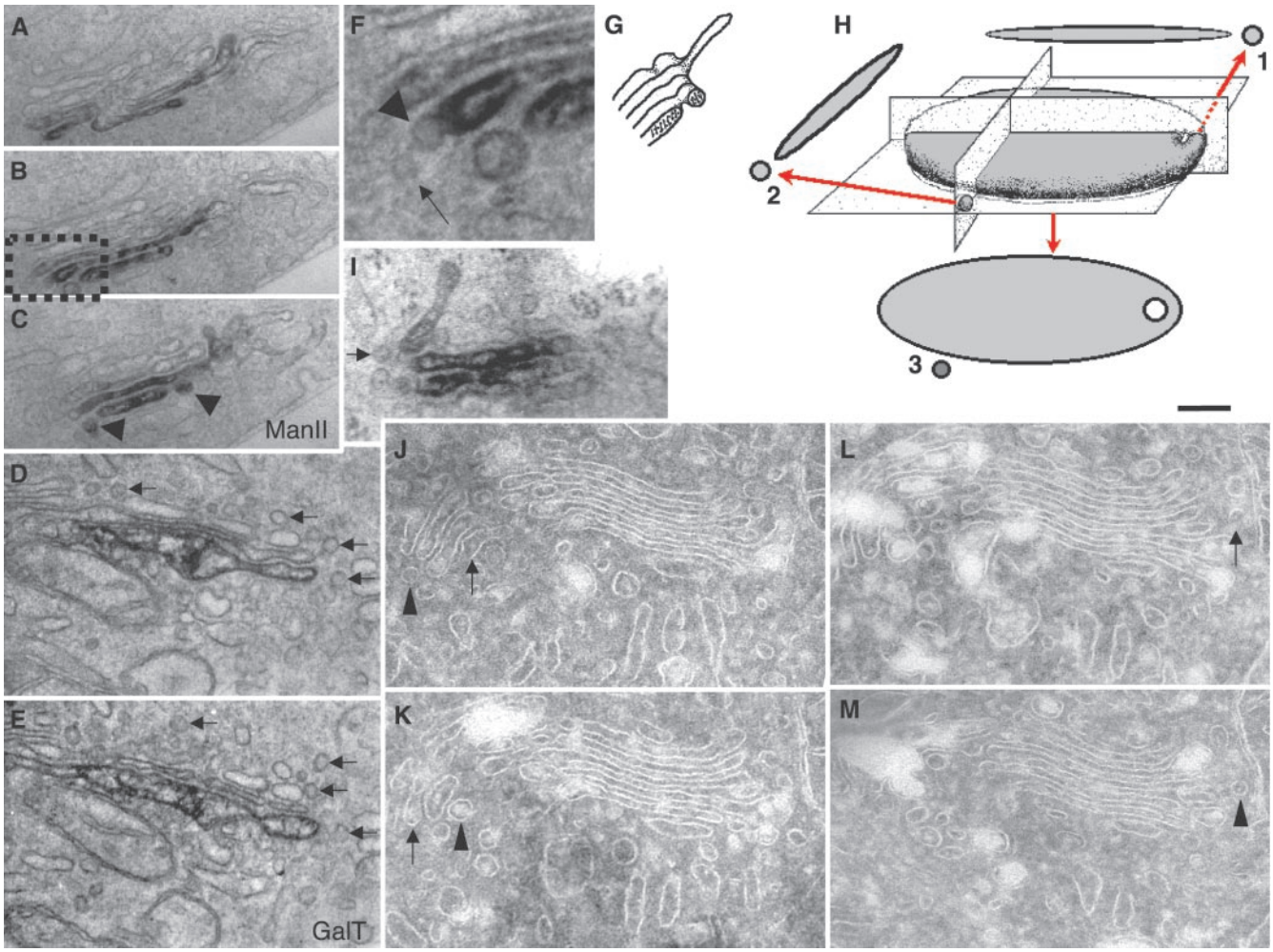

Figure 2. Golgi enzymes are excluded from buds and 50- to 60-nm vesicles and buds at steady state. RBL cells (A–C, F, and I), human fibroblasts (D and E), and NRK cells (J–M) were prepared for immunoperoxidase (A–F and I) EM labeling of Golgi enzymes, or they were cryosectioned (J–M). Man II (A–C, F, and I) and GalT (D and E) are excluded from round profiles (D and E, arrows) and COPI buds (F, arrowhead). Some round profiles in the vicinity of the Golgi-enzyme-positive cisternae (C, arrowheads) seen in serial sections (A–C) as a cross section of perforated zones (see scheme in G). (F) Enlargements of areas indicated by the black box in B. After membrane permeabilization with 0.1% Triton X100 (I), ManII is still absent in round profiles (arrow), although the preservation of Golgi ultrastructure is poor. In H, a scheme shows how near-rimmal round profiles can derive from cross sections of the cylinder-like cisternal rim around near-rimmal pores (1) or from actual vesicles (2) in cross sections (1 and 2) or in tangential sections (3). In J–M, perforated zones analyzed by serial cryosections; a substantial proportion of the round profiles (arrowheads) located in the vicinity to cisternal rims seen as cross sections of tangential tubules or perforated zones of cisternae (arrows). Bars, 300 nm (A–C); 200 nm (D, E, I, and J–M); and 120 nm (F).

Finally, we used the preembedding nanogold technique followed by gold-enhancement (see *Materials and Methods*) for the 3D labeling of GalT, ManI-FP, STF, and ManII (Figure 4, A–H). Gold particles marking these Golgi enzymes were seen over Golgi cisternae, as expected, but not over peri-Golgi round profiles (Tables 1 and 2). In tangential sections, a concentration of these Golgi enzymes (and especially ManII; Figure 4C) was observed within perforated zones of Golgi cisternae. These samples also were examined in three dimensions in thick, 200-nm sections tilted from +60 to −60 degrees at 1° increments while acquiring a series of consecutive projections (tilting analysis; see *Materials and Methods*). These tilt series were analyzed directly, without tomographic reconstruction, because shadows around the gold-enhanced nanogold particles hamper the analysis of such reconstructions. This tilting analysis allows true vesicles (profiles preserving a round shape during the whole cycle of tilting) to be distinguished from other structures, and in particular the detection of vesicles labeled for β-COP (Figure 4, D–F). However, there were no gold particles marking the enzymes that colocalized with true vesicles (profiles preserving a round shape during the whole cycle of tilting; unpublished data), confirming that vesicles were not labeled. To bypass the membrane penetration problem and avoid the need for permeabilization, we used an antibody against the cytosolic tail of GalT. Again, gold particles were associated with cisternae and tubules, and not with round profiles (see *Materials and Methods*) and buds (Figure 4A and Table 2). Thus, both the immunoperoxidase and nanogold preembedding techniques indicate the exclusion of Golgi enzymes from 50- to 60-nm peri-Golgi vesicles. In conclusion, several experimental approaches concur to indicate

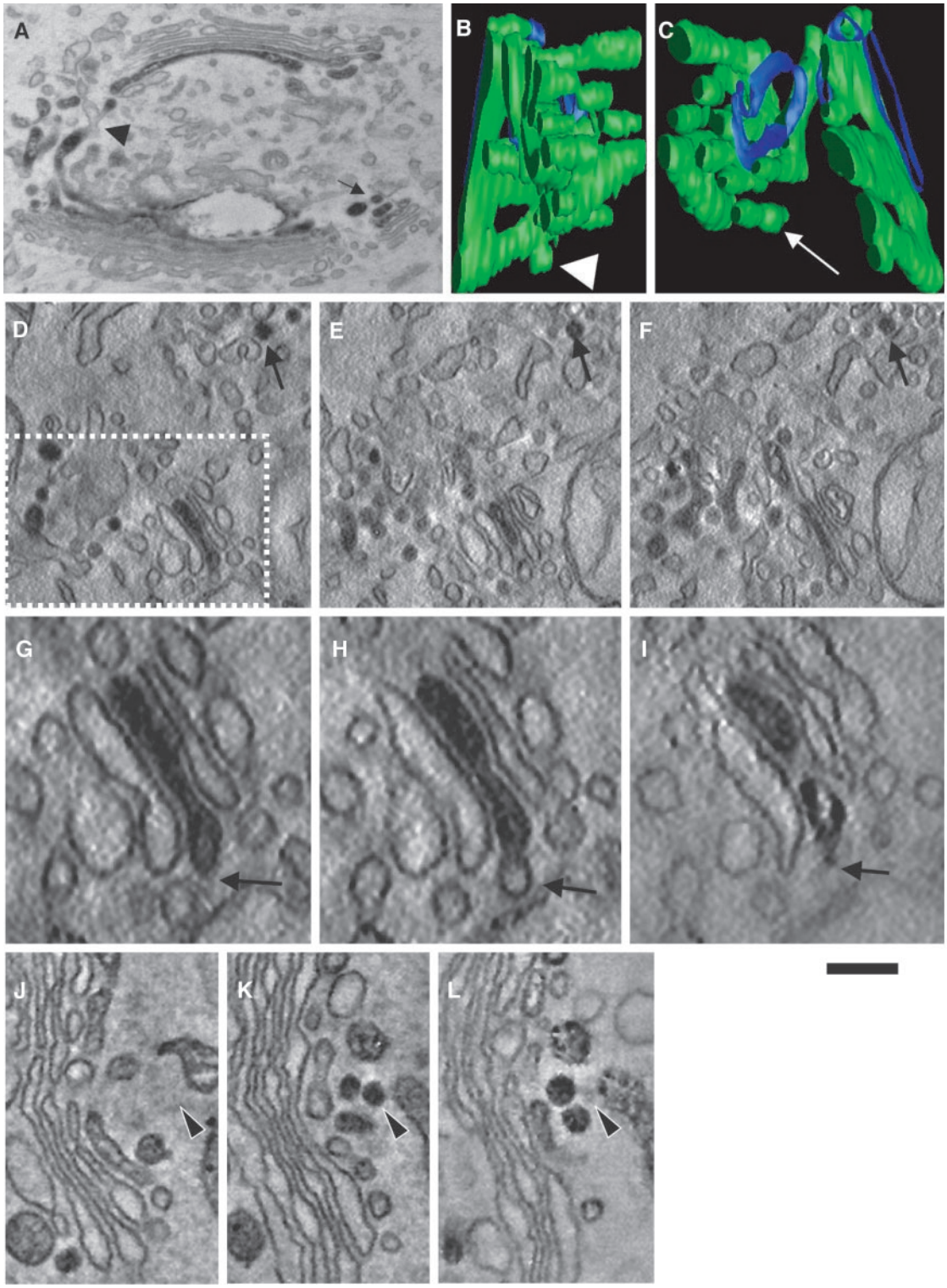

Figure 3. STF-HRP is absent in 50- to 60-nm round profiles and cisternal buds. NRK cells stably transfected with STF-HRP (A–I) or COS7 cells (J–L) transiently transfected with a ssHRP^{KDEL} construct (as a positive control) were prepared for immunoperoxidase EM (A) and subjected to EM tomography (B–L). (A) Round profiles filled with DAB precipitate (arrow) and connections (arrowhead) between STF-positive and SFT-negative Golgi membranes are visible on 50-nm routine cross sections. (B–L) Electron tomography. (B and C) Three-dimensional reconstruction and surface rendering of the DAB-positive membranes from the white dashed box in D reveal that DAB-positive vesicles (spheres isolated from other membranes) are not present in the Golgi area. Instead, round profiles often represent sections of cylinders with a DAB-positive part (green) connected with DAB-negative structures (blue). Virtual 5-nm sections were taken from the surfaces (D, G, and J), the middle (E, H, and K), and the bottom (F, I, and L) of these thick 200-nm sections. (D–F) Serial round profiles (arrow) filled with STF-HRP that indicate that these represent cross sections of an STF-positive tubule. (G–I) Empty cisternal bud (arrow). (J–L) Actual vesicle filled with ssHRP^{KDEL} (arrowhead). Bars, 300 nm (A); 120 nm (B and C); 200 nm (D–F); 100 nm (G–I); and 150 nm (J–L).

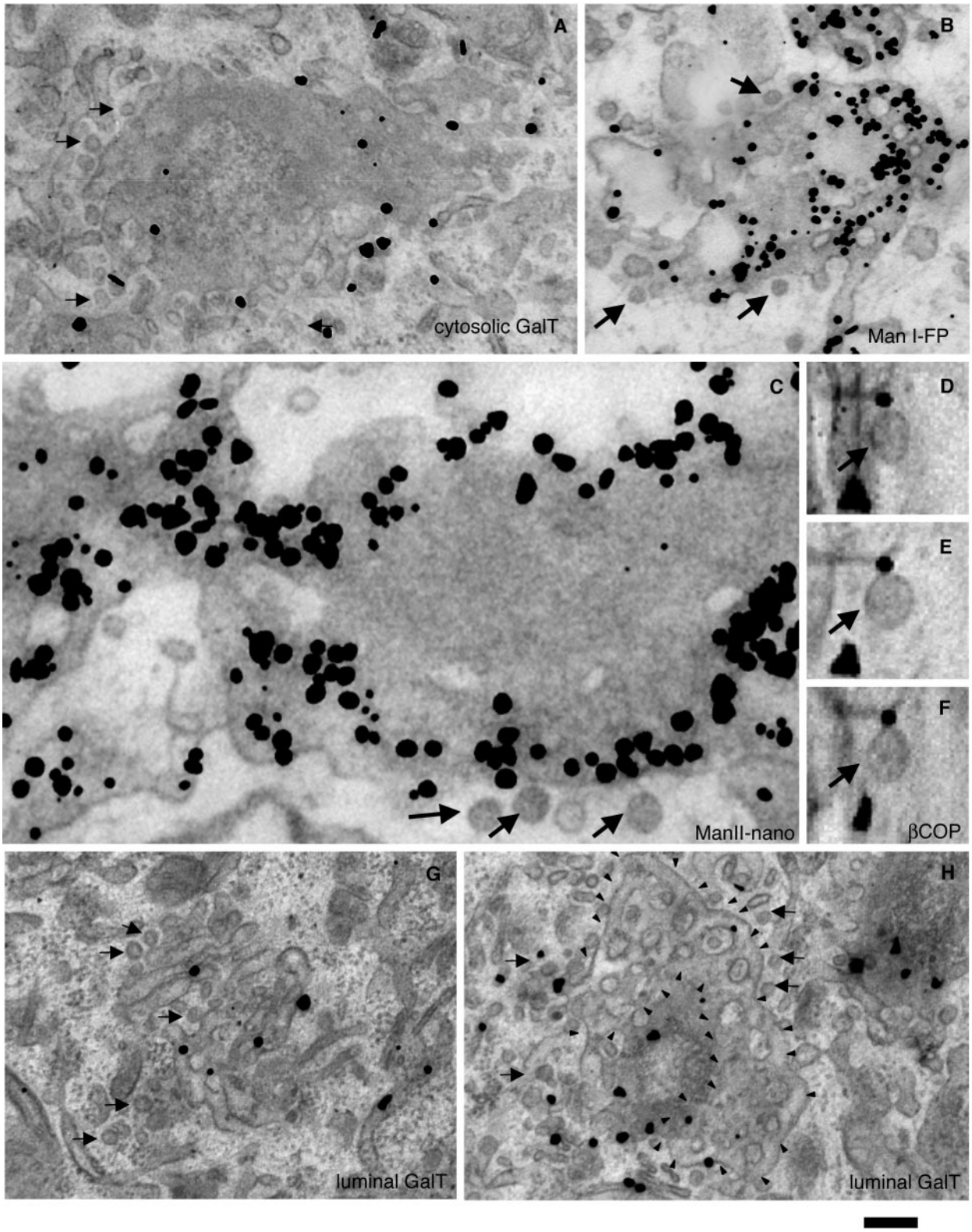

Figure 4. At steady state, Golgi enzymes are depleted from peri-Golgi vesicles but are enriched in perforated zones of cisternae. Human fibroblasts (A, G, and H), and COS7 (B) and NRK (C and D–F) cells were prepared for immuno-nanogold labeling (A–C, G, and H; see *Materials and Methods*), sometimes with the subsequent tilting of thick sections (D–F). GalT (A, G, and H), ManI-FP (B), and ManII (C) are depleted from 50- to 60-nm vesicles visible in tangential sections. Anti-β-COP labeling is present on actual vesicles (D–F), which look round at different angles (50° in D, 0° in E, and −50° in F). The detection of GalT in vesicles does not depend on poor permeabilization of vesicular membranes because it is observed when an antibody against the cytosolic epitope of GalT is applied (A). Arrows indicate actual vesicles. In H, small arrowheads indicate limits of perforated zones which derive from the GalT-negative cisterna. Bars, 300 nm (A, G, and H); 200 nm (B); 100 nm (C); and 70 nm (D–F).

Table 2. Relative LDs of GalT in human fibroblasts at steady state and during synchronous transport of PC and VSVG (miniwave protocol, nanogold-gold enhancement technique)

Condition/protocol, Ab against, (n)				LD [% cisternae (±SE)]		
				Non-perforated parts of cisternae	Perforated parts of cisternae	Vesicle profiles[b]
Steady state		Luminal GalT	(30)	100.0 (±15.4)	216.2 (±20.6)[d]	8.8 (±5.1)[c]
		Cytosolic GalT	(54)	100.0 (±17.1)	206.5 (±22.0)[d]	8.9 (±5.7)[c]
Miniwave[a]	0 min	Cytosolic GalT	(31)	100.0 (±14.2)	259.3 (±16.7)[d]	7.5 (±5.2)[c]
	7 min	Cytosolic GalT	(33)	100.0 (±15.3)	117.1 (±18.0)	7.1 (±4.1)[c]

See Table I legend for further details.

[a] Miniwave, 40°C (3 h); 15°C (15 min); 40°C (0/7 min), see *Materials and Methods*.

[b] See *Materials and Methods* for definition of vesicles on tangential sections.

[c] Significantly different ($p \leq 0.01$) from cisternae.

[d] Significantly different ($p \leq 0.05$) from cisternae.

that 50- to 60-nm peri-Golgi vesicles and cisternal buds with a COPI-like coat are depleted of Golgi enzymes.

Blockage of Membrane Fusion Does Not Lead to the Appearance of 50- to 60-nm Vesicles Filled with Golgi Enzymes

A possible reason for failing to observe COPI vesicles carrying Golgi enzymes would arise if there exists a subpopulation of peri-Golgi vesicles that contain Golgi enzymes but that is too transient to be seen using our traditional experimental setup. To overcome this problem, we reasoned that if COPI vesicles containing Golgi enzymes normally form, but fuse immediately with the acceptor cisterna, if fusion is inhibited, they should accumulate and hence become detectable. To block membrane fusion along the secretory pathway, we applied two approaches: microinjection of the His6-α-SNAP (L294A) mutant, which is unable to disassemble SNARE complexes (Barnard *et al*., 1996; Band *et al*., 2001); and *N*-ethylmaleimide (NEM) treatment (Mironov *et al*., 2001). First, NRK cells stably expressing STF-HRP were microinjected with the α-SNAP mutant, and then (20 min after microinjection) prepared for immuno-EM. Many 50- to 60-nm vesicles accumulated in the Golgi area, but they were depleted of STF-HRP after detection of STF with either DAB (Figure 5A) or nanogold (Figure 5, B and C). To allow morphometric analysis of a large cell population (where microinjection is not feasible), we blocked fusion by treating cells with NEM under well-characterized conditions (Mironov *et al*., 2001). We then prepared cryosections and determined the concentration of GalT in the resulting vesicles (Figure 5D). As expected (Mironov *et al*., 2001), Golgi round profiles increased in number to levels 2.5-fold higher than basal values (Table 3), confirming that NEM had inhibited vesicle fusion. However, again, these peri-Golgi round profiles were depleted (4.5-fold) of GalT (Table 3). Thus, we find no evidence for a transient subpopulation of COPI-coated vesicles that are rich in Golgi enzymes.

To test whether the 50- to 60-nm vesicles that accumulated in the Golgi area after microinjection of His6-α-SNAP are COPI dependent, we blocked the COPI machinery by microinjection of an inhibitory polyclonal anti-β-COP antibody that inhibits the formation of COPI vesicles (Pepperkok *et al*., 1993) and prepared these cells for correlative light-EM (Polishchuk *et al*., 2000). We hypothesized that if the formation of 50- to 60-nm vesicles in the Golgi area is COPI dependent, then under these conditions (when the formation of COPI vesicles is inhibited) the simultaneous block of their fusion with cisternae would not affect their number. The anti-β-COP antibody induced the expected tubulation of the Golgi (Pepperkok *et al*., 1993) and disappearance of 52-nm vesicles (Figure 5F). When His6-α-SNAP was microinjected together with this antibody, 52-nm vesicles did not accumulate in the same way as seen when His6-α-SNAP was microinjected alone (Figure 5, A–C, and Table 1), and the structure of the Golgi was preserved (Figure 5E). Thus, 50- to 60-nm vesicles formed in the presence of His6-α-SNAP or NEM are COPI dependent.

COPI Vesicles Generated in a Cell-free System Are Depleted of Golgi Enzymes

As noted above, small membrane fragments (assumed to represent bona fide COPI vesicles) enriched in Golgi enzymes have been isolated in vitro after incubation of isolated Golgi membranes with cytosol and GTP (Lanoix *et al*., 1999). We assessed whether all of these small membranes represent COPI-dependent, 50- to 60-nm vesicles. First, we tested whether our control isolated Golgi membranes (Figure 6A) contained 50- to 60-nm vesicles. Electron tomography revealed that most of the round profiles (Figure 6B, arrows) visible in single sections represented cross sections of tubules (Figure 6C, white arrow). Then, using the same cell-free assay as that described by Lanoix *et al*. (1999) (with minor modifications; see *Materials and Methods*), we incubated Golgi membranes with cytosol, GTP, an ATP-regenerating system in a K^+-rich transport buffer containing Ca^{2+}. Under these conditions, and especially when His6-α-SNAP was added to the incubation mixtures, an accumulation of 50- to 60-nm vesicles (arrowheads) near cisternae (arrows) were observed (Figure 6D). To test whether this generation of 50- to 60-nm vesicles in the presence of His6-α-SNAP is COPI dependent, we replaced normal cytosol with COPI-depleted cytosol. As expected (Misteli and Warren, 1994), under these conditions most of the Golgi cisternae were transformed into tubular networks without vesicles, as visible after tomographic reconstruction (Figure 6E) and thin sectioning (Figure 6F). Incubation of Golgi membranes with COPI-depleted cytosol and His6-α-SNAP partially prevented the tubulation of the Golgi (Figure 6G). Addition of a cytosol fraction enriched in COPI to the COPI-depleted cytosol restored the generation of 52-nm vesicles in the presence of His6-α-SNAP (unpublished data). Next, we isolated a similar light fraction of Golgi membranes (to that

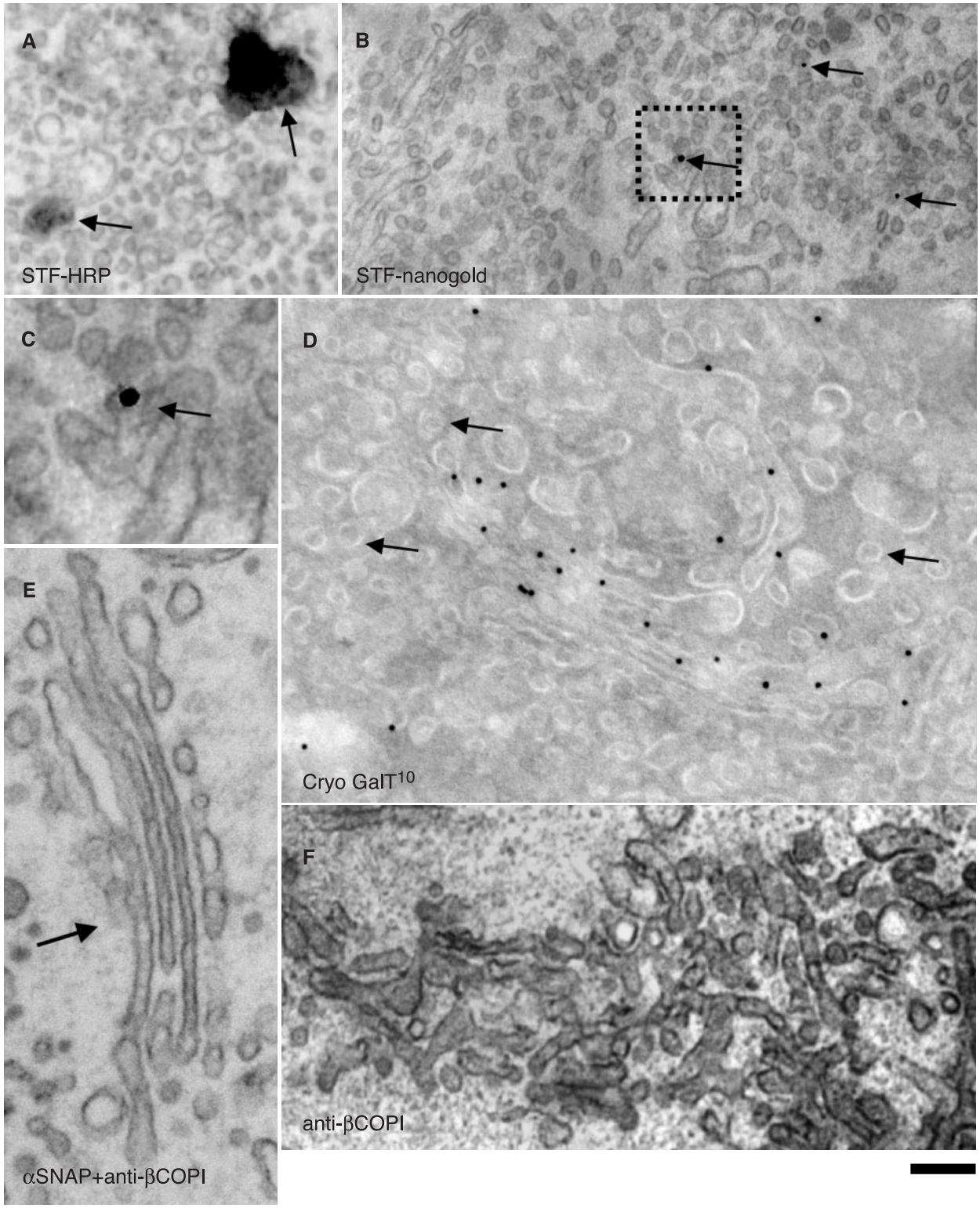

Figure 5. Block of the SNARE machinery does not induce the appearance of Golgi enzymes in COPI vesicles. NRK cells stably transfected with STF-HRP (A–C) were microinjected with the His6-α-SNAP mutant. Human fibroblasts (D) were treated with NEM (100 μM, on ice for 15 min; see *Materials and Methods*). NRK cells were microinjected either with a mixture of His6-α-SNAP and a polyclonal anti-β-COP antibody (E) or with only the anti-β-COP antibody (F). The cells were then prepared for immonoperoxidase (A), immuno-nanogold (B and C), and cryoimmuno-gold (D) EM labeling, or for routine EM (E and F). The blocks of the fusion machinery led to the accumulation of round profiles depleted of Golgi enzymes. DAB-staining (A, arrows), nanogold (B and C, arrows), and 10-nm gold (D, arrows indicate empty vesicles). (C) Enlargement of the area presented inside the black box in B. The anti-β-COP antibody induced tubulation of the Golgi (F), but prevented Golgi (E, arrow) alteration and formation of COPI vesicles under the action of the His6-α-SNAP mutant (E). Bar, 220 nm (A and B); 70 nm (C); 80 nm (D); and 150 nm (E and F).

Table 3. Relative LDs of GalT in human fibroblasts: NEM treatment

Treatment (n = 25)	LD [% cisternae (±SE)] Cisternae	Peri-Golgi RPs	Total RPs
−NEM	100.0 (±60.0)	25.9 (±31.8)	217
+NEM (100 μM, on ice for 15 min)	100.0 (±60.5)	22.1 (±29.1)	550

RP, round profile. See Table 1 legend for details.

described by Lanoix *et al*., 1999) that on routine EM sections exhibited roundish profiles with diameters ranging from 40 to 150 nm and a high proportion of 50- to 60-nm round profiles (Figure 6, H–P). Most of these were 50- to 60-nm vesicles, although at the bottom of the pellet (Figure 6H, left) the proportion of cisternal fragments, which often looked invaginated, was higher (Figure 6, I and J). In contrast, at the top of the pellet (Figure 6H, right, K, and L), the proportion of 50- to 60-nm round profiles was higher. When we isolated the light fraction after the use of COPI-depleted cytosol, we obtained a much less abundant light fraction that contained mostly short tubular fragments, and almost no 50- to 60-nm vesicles (unpublished data). The enzyme content of the various membrane fractions was then examined. Cryoimmunolabeling of the light fraction detected ManII mostly over cisternal fragments, and not >50- to 60-nm vesicles (Figure 6, M–P). The level of ManII exclusion from 50- to 60-nm vesicles was ~2.6-fold (Table 4), similar to our data obtained in situ (Table 1). The LD of ManII over cisternal fragments was 1.5 times higher than that over all Golgi cisternae in the initial isolated Golgi membranes (Table 4). Thus, the 50- to 60-nm vesicles formed in a COPI-dependent manner in this cell-free assay are depleted of Golgi enzymes.

To understand why Lanoix *et al*. (1999) obtained Golgi enzyme enrichment (per unit of membrane surface area) in the same light fraction, we compared the concentrations of ManII in the light fraction and in the original fraction of isolated Golgi membranes. To this end, we exploited two approaches. Initially, we measured the absolute volume of the vesicular pellet. Then, we estimated the absolute surface area of cisternal fragments and 50- to 60-nm COPI vesicles (see *Materials and Methods*). Our estimates revealed that the mean fraction of Golgi cisternae in the original Golgi membranes was 23%. To distinguish actual 50- to 60-nm vesicles from tubules of the same diameter, we used serial sections (Figure 6, I–L); these revealed that ~40% of the 50- to 60-nm round profiles actually represent cross sections of short tubules. The LD of ManII over all membranes of the light fraction seemed to be twofold higher than that over all of the membranes of the original isolated Golgi fraction. The second approach was based on an assessment of ManII concentrations by using Western blotting. The optical density of blot staining per unit of surface area of all of the membranes was estimated from the integrated blot densities (Figure 6Q). Although, the latter are very similar, due to the different concentrations of Golgi cisternae (in the pellet of the original Golgi membranes) and their fragments (in the light fraction) the blot-density per unit of all-membrane surface area for the light fraction was 2.9-fold higher than that for the original Golgi membranes (1726 arbitrary units: 45.5 μm^{-2} = 37.9 $\times$ 10^{-6} arbitrary units $\cdot$ μm^{-2} vs. 1328 arbitrary units: 102.2 μm^2 = 13.0 $\times$ 10^{-6}, respectively). Thus, our data confirmed once more that ManII is excluded from COPI vesicles forming in vitro, whereas it is enriched in the light fraction, in agreement with data by Lanoix *et al*. (1999). However, we have revealed that this enrichment is not due to the concentration of ManII in COPI vesicles, but to the higher purity of Golgi membranes and vesicles, which are actually again depleted of Golgi enzymes, in the light fraction.

Golgi Enzymes Are Enriched in Perforated Zones of Cisternae

To examine whether the perforated zones of Golgi cisternae are sites of Golgi enzyme concentration, we first used tangential sectioning of Golgi stacks. The images generated from these sections contained not only the solid parts of the cisternae but also their perforated zones and tubules connecting neighboring stacks (Ladinsky *et al*., 1999). These tangential sections demonstrated that intense labeling was often present in the perforated zones (mostly at the rims) of Golgi cisternae (Figure 4, A–C). By using antibodies against either the luminal or the cytosolic domains of GalT with tangential sections, 50- to 60-nm vesicles (see *Materials and Methods*) were found to be depleted of GalT (Figure 4, G and H, and Table 2). This confirms that bona fide vesicles exclude Golgi enzymes and suggests that Golgi enzymes are preferentially concentrated in perforated areas near the rims of the cisternae. Moreover, within a single cisterna, Golgi enzymes are more concentrated in the peripheral perforated areas than in the cisternal core.

Next, we examined whether the enzyme distribution depends on the functional state of the secretory system. To this end, cargo movement through the Golgi was synchronized. Human fibroblasts and RBL cells were infected with the 045 strain of VSV, with the human fibroblasts also being stimulated to synthesize PC (Mironov *et al*., 2001). Cargo was then accumulated in the ER and then in the intermediate compartment, according to our previously described "small-pulse synchronization" protocol (see *Materials and Methods*). Just before initiation of intra-Golgi transport, the labeling density of GalT in tangential sections was much higher over the perforated zones than over the core of the cisternae; however, this difference was virtually abolished within 7 min of the release of the transport block (Table 2, cytosolic antibody).

Because it is difficult to examine tangential cryosections quantitatively, we set up methods to identify perforated areas of cisternae in cryo-cross sections (Figure 2, I–N). To this end, we compared the distribution of gold particles over these perforated zones (cisternal rims with attached near-rimmal round profiles) with their distribution over nonperforated zones (cisternal rims without near-rimmal round profiles) (Figure 7A) both before and after the release of the transport block. Before the release (0 min), the average distance between gold particles and a rim in perforated zones was 112.6 nm, more than twofold less than in nonperforated zones (299.4 nm; $p \leq 0.05$), indicating that GalT was more concentrated near the cisternal rims, where the cisternal perforations were situated. After release of the traffic block, however, this difference was no longer significant (Table 5), illustrating that the asymmetric distribution of GalT within a cisterna is lost upon release of the traffic block.

In an alternative approach, we divided cisternae along their length into three portions: one-fourth with attached near-rimmal round profiles, typical of the perforated zones; the middle one-half or cisternal core; and one-fourth without near-rimmal round profiles, typical of the nonperforated zones. We then estimated the LDs for GalT over these three

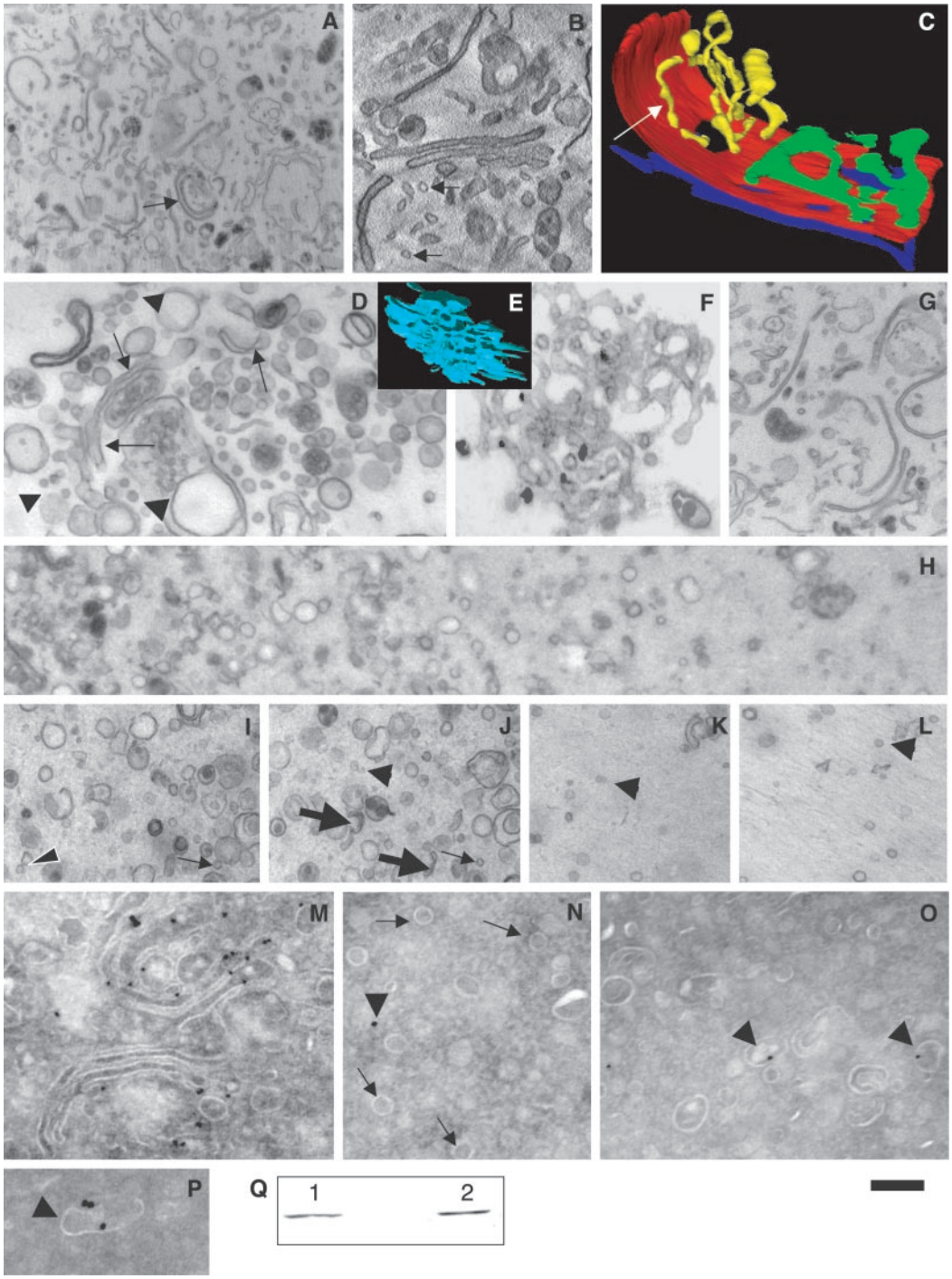

Figure 6. COPI-dependent vesicles isolated after incubation of Golgi membranes with cytosol in a cell-free assay are depleted of ManII. Golgi membranes (A, arrow) isolated from rat liver were examined immediately after isolation (A–C and M), and after an incubation with GTP, an ATP regeneration system and ordinary cytosol in a K^+-rich buffer in the presence of the His6-α-SNAP mutant (D), or COPI-depleted cytosol (E and F), or COPI-depleted cytosol and His6-α-SNAP (G). The light fraction of Golgi membranes was isolated (H–L and N–P) after incubation of the Golgi membranes with the different mixtures. The samples were examined by routine EM (A, D, and F–L), electron tomography (virtual 5-nm section in B, surface rendering in C and E) or cryoimmuno-gold EM (M–P), and by Western blotting by using an antibody against ManII (Q). In M, isolated Golgi cisternae were labeled for ManII (10-nm gold). In Q, ManII labeling was seen both in the diluted Golgi membranes (1) and in the light fraction (2) (see *Materials and Methods*). In most cases, round profiles (B, arrows) visible in original isolated Golgi membranes occurred as tubules (C, white arrow). The pellet of the light Golgi fraction contained a mixture of 50- to 60-nm vesicles (I–L, arrowheads), tubules (I and J, thin arrows), and short cisternal fragments (J, thick arrows) at the bottom (left side of H, and in I and J), and at the top (right side of H and in K and L), mostly loosely packed 50- to 60-nm vesicles (K and L, arrowheads). Labeling for ManII is present mostly over the cisternae (M) and cisternal fragments (O and P, arrowheads), and not over vesicles (N, arrows). The arrowhead in N is background labeling. I and J and K and L are serial sections, allowing 50- to 60-nm vesicles (I–L, arrowheads) to be distinguished from cross sections of 50- to 60-nm tubules (I–J, thin arrows). Bars, 900 nm (A); 260 nm (B–F and I–L); 600 nm (G); 450 nm (H); and 200 nm (M–P).

Table 4. Relative LDs of ManII in isolated Golgi membranes

Samples (n = 25)	LD [% cisternae (±SE)]		Total volume (μm^3)
	Cisternae	RPs	
Isolated Golgi	100.0 (±37.3)	38.1 (±14.8)	0.003
Light fraction	100.0 (±41.4)	26.2 (±17.1)	0.005

RP, round profile. See Table 1 legend for details.

portions. Table 5 shows that just before the release of cargo (0 min) from the intermediate compartment (where cargo accumulates during the 15°C block, according to the miniwave protocol; see *Materials and Methods*), the LD of GalT over perforated zones was 6.5-fold higher than that over the cisternal core and the nonperforated zones (281 vs. 43%) (Table 5). The same measurement was carried out after the initiation of intra-Golgi transport, during the passage of a cargo wave through the stacks, according to the maxiwave protocol (7 and 18 min after the shift from 15 to 40°C; see *Materials and Methods*). Under these conditions, the asymmetry in the GalT distribution along the Golgi cisternae decreased (Table 5). These data suggest once more that in quiescent Golgi stacks, Golgi enzymes are preferentially distributed in peripheral perforated areas of cisternae, whereas in stacks actively engaged in traffic, the lateral distribution of Golgi enzymes becomes more homogeneous within the cisternae.

Because previously published results were obtained in nonsynchronized cells (Martinez-Menarguez *et al.*, 2001; Cosson *et al.*, 2002), we examined Golgi enzyme distribution in cisternae under steady-state transport conditions, i.e., when VSVG and PC were constantly moving through the Golgi (4 h after infection of human fibroblasts with tsVSV, incubated at 32°C in the presence of ascorbic acid). Under these conditions, there was also a clear asymmetry in the Golgi enzyme distribution within Golgi cisternae (Figure 7, C–E), although it was less pronounced than that in resting cells in which transport was blocked. Thus, the distribution of Golgi enzymes under steady-state transport conditions represents an intermediate situation between quiescent Golgi (0 min) and maximal transport activity (18 min).

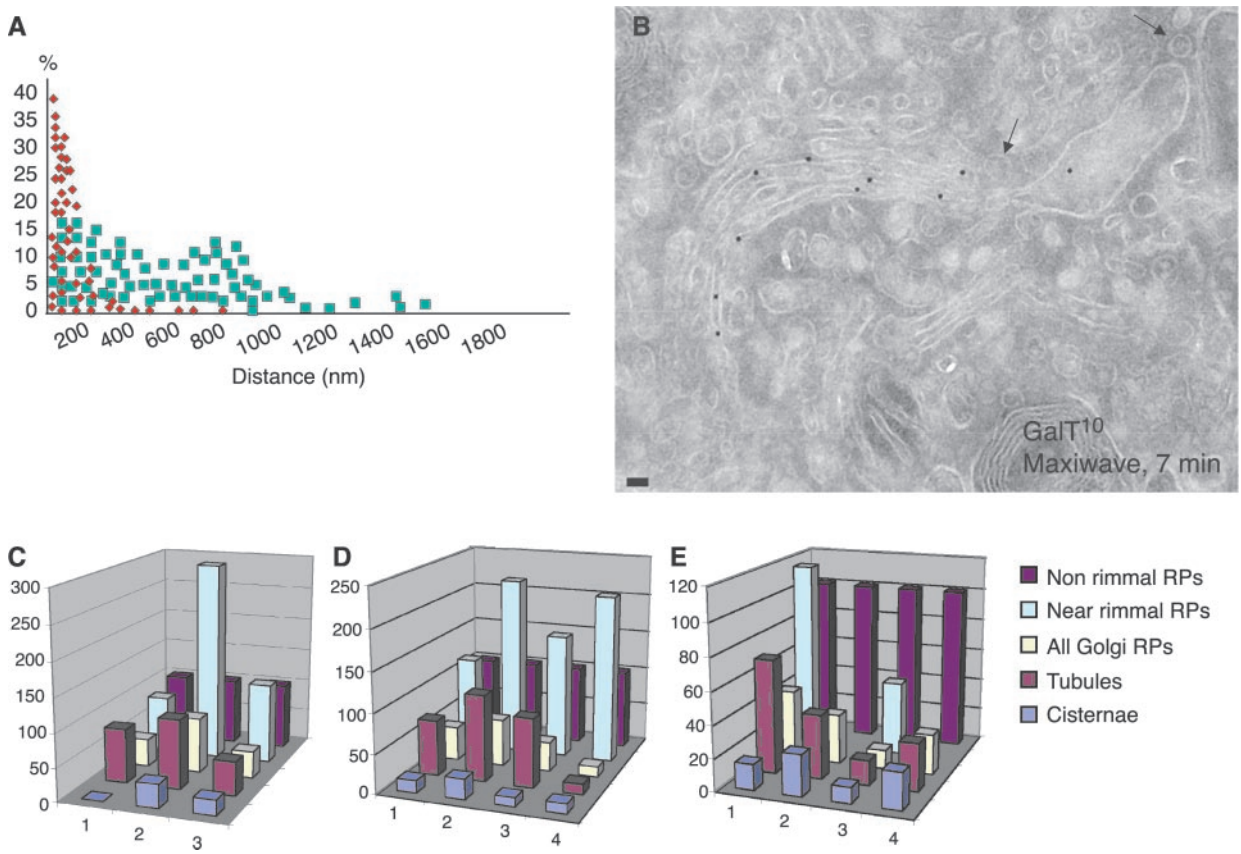

Figure 7. Distribution of Golgi enzymes over different profiles during cargo passage through the Golgi. Analysis of cryosections. Immunogold labeling of GalT in human fibroblasts (A, B, D, and E) and ManII in RBL cells (C). (A) Distribution of gold particles (from 30 samples) related to the perforated zones (cisternal rims with attached near-rimmal round profiles, red squares) versus the distribution of gold particles related to the nonperforated zones (rims without near-rimmal round profiles, green squares). GalT was substantially enriched (the average distance is shorter) within the rims with attached near-rimmal round profiles. (B) Nonrimmal round profiles remained depleted of GalT (arrows). (C–E) Graphs showing the LDs of ManII (C) and GalT (D and E) over different Golgi profiles during the transport of PC and VSVG through the Golgi in cells subjected to the maxiwave (B, D, and E) and miniwave (C) protocols (see *Materials and Methods*). 1, at 40°C; 2, after the 15°C block; 3, 7 min after the release of the 15°C block; and 4, 12 min after the release of the 15°C block. All data are normalized considering the LD over cisternae as 100%. All LD values for the nonrimmal round profiles are significantly different ($p \leq 0.05$) from those of the cisternae. Bar, 80 nm (B).

Table 5. Relative LDs of GalT in human fibroblasts after alignment of cisternae in relation to the attached near-rimmal RPs, at steady state, and during synchronous movement of PC and VSVG (maxiwave protocol)

Condition/protocol (n)			LD [% cisternae (±SE)]		
			1/4 with a near-rimmal RP	2/4 (Middle)	1/4 w/o a near-rimmal RP
Steady state		(30)	140.5 (±6.9)	81.1 (±3.0)[a]	97.3 (±6.5)[a]
At 40°C		(30)	209.0 (±8.8)	65.7 (±3.3)[a]	59.7 (±5.5)[a]
Maxiwave[c]	0 min	(30)	281.1 (±10.9)	37.8 (±4.9)[a]	43.2 (±6.9)[a]
	7 min	(30)	118.7 (±8.8)	92.3 (±7.3)[b]	96.7 (±9.6)[b]
	18 min	(30)	101.2 (±5.3)	91.6 (±6.1)[b]	115.7 (±6.1)[b]

[a] Significantly different ($p \leq 0.05$) from 1/4 with a near-rimmal RP.

[b] Not significantly different ($p > 0.05$) from 1/4 with a near-rimmal RP.

[c] Maxiwave, 40°C (3 h) 15°C (2 h); 40°C (0/7/18 min), see *Materials and Methods*.

RP, round profile. See Table 1 legend for further details.

As a final test for the asymmetric distribution of Golgi enzymes within Golgi cisternae, we assessed their LDs over near-rimmal round profiles located within 40 nm of cisternal rims, reasoning that if the perforated zones are enriched in Golgi enzymes, the LDs over near-rimmal round profiles should be higher than the overall LD of peri-Golgi round profiles. Table 1 shows that, indeed, the LDs of Golgi enzymes over these near-rimmal round profiles are almost always higher than the overall LD of peri-Golgi round profiles, and in some cases even higher than that over all cisternae. This means that concentration of Golgi enzymes in perforated zones of Golgi cisternae is so high that even the presence of 60% of actual vesicles (that are depleted of Golgi enzymes) in this mixture of peri-Golgi round profiles does not result in a lower mean concentration of Golgi enzymes than that in cisternae. Similarly, during synchronous transport of cargo through the Golgi, the LDs of GalT (Figure 7B) and ManII (Figure 7C) over the nonrimmal round profiles remained consistently low, whereas those over the near-rimmal round profiles, where Golgi enzymes have accumulated, decreased after the arrival of cargo. Clearly, if peri-Golgi round profiles are simply assumed to represent peri-Golgi vesicles, then the accumulation of Golgi enzymes in perforated zones under steady-state or resting conditions easily leads to a large overestimation of Golgi enzyme concentrations in COPI vesicles. These data suggest that Golgi enzymes are distributed asymmetrically along a cisterna, because they are concentrated in perforated zones at the rims of Golgi cisternae.

DISCUSSION

Golgi Enzymes Are Excluded from COPI-dependent Golgi Vesicles

Our main conclusion is that peri-Golgi vesicles are deprived of Golgi enzymes. This conclusion is in agreement with the exclusion of ManII from peri-Golgi round profiles described by Orci and colleagues (Cosson *et al*., 2002), but at variance with the earlier data of Martinez-Menarguez *et al*. (2001). The latter study showed an enrichment of ManII in COP-coated peri-Golgi round profiles, which were assumed to represent peri-Golgi vesicles. However, the presence of a COPI-like coat, which was used by Martinez-Menarguez *et al*. (2001), is not a specific feature of COPI-dependent peri-Golgi vesicles (Figure 1A). A COPI-like coat is found mostly on the rims of Golgi cisternae, and especially on rims where adjacent perforations are found, and on tangential tubules emanating from a single cisterna (Weidman *et al*., 1993; this study), rather than on 50- to 60-nm vesicles. Moreover, Golgi-derived tubules are labeled for COPI (Rojo *et al*., 1997; this study). Furthermore, COPI-coated buds can occur as round profiles during sectioning. Although we have confirmed that under specific experimental conditions, peri-Golgi round profiles can be enriched in ManII (Table 1 and Figure 7C), our 3D analyses clearly show that round profiles rich in Golgi enzymes represent cross sections of peri-Golgi tubules and perforated zones of cisternae. In contrast, actual vesicles are depleted of Golgi enzymes. Finally, we have confirmed that COPI vesicles formed under cell-free assay conditions also are depleted of ManII. At the same time, the differences we see between ManII-FP in COS7 cells and endogenous ManII in NRK cells could be due to the higher levels of ManII-FP expression, because this can affect the level of its depletion from buds and vesicles, and can induce a higher level of Golgi tubulation (unpublished observations) and thus an enrichment of tubule cross sections (containing a higher density of ManII-FP) in the round profiles.

What then is the mechanism responsible for the exclusion of Golgi enzymes from COPI-dependent vesicles? It seems unlikely that an interaction between COPI and Golgi enzymes participates in this process (Dominguez *et al*., 1998). A more likely scenario would involve the oligomerization of Golgi enzymes within the cisternal domains of the Golgi, e.g., either self-aggregation due to low pH, or oligomerization driven by the association with cargo during glycosylation. Large oligomers may not be able to be included in highly curved (with double-axial curvature) COPI-coated domains and vesicles. In an earlier study, we showed that small cargo proteins and large protein aggregates can traverse the Golgi by a common mechanism without entering peri-Golgi vesicles (Mironov *et al*., 2001). Both cargo proteins and Golgi enzymes could be excluded from peri-Golgi vesicles by the same mechanism. More work is needed to elucidate the mechanisms by which Golgi enzymes, and probably most cargo proteins, are excluded from COPI vesicles.

Perforated Zones of Golgi Cisternae and peri-Golgi Tubules Are the Sites of Golgi Enzyme Concentration

The second key conclusion of the present study is that Golgi enzymes are enriched in perforated zones of cisternae. This conclusion is supported by several observations. First, in tangential sections of Golgi cisternae, the concentration of Golgi enzymes is higher in perforated zones than in the central parts of cisternae, both during steady-state transport and when all cargo movement is blocked. Second, the concentration of Golgi enzymes is also not uniform in cross sections of cisternae but forms a significant gradient along the cisternal length. Finally, by plotting the number of gold particles as a function of the distance to the cisternal rim, the highest concentrations of Golgi enzymes are found at perforated cisternal rims. The largest accumulation of Golgi enzymes near perforated cisternal rims is observed in synchronized cells before the release of the temperature block, i.e., when there is virtually no transport of cargo proteins through the Golgi complex. After the release of the temperature block, when a significant fraction of cargo-containing membranes has arrived at the Golgi, this asymmetric distribution of Golgi enzymes decreases, potentially due to a reorganization of the Golgi cisternae. However, as soon as the transport wave has passed and as the relatively slow steady-state transport conditions are reached, the Golgi enzymes again accumulate in perforated zones.

Tangential sections of the Golgi reveal that the near-rimmal position of Golgi vesicles is common. In our samples, ~30% of the round profiles visible within 40 nm of the cisternal rims represent cross sections of tangential tubules or perforated zones of cisternae, whereas 70% are true vesicles (Figure 2, I–N). In agreement with this, when we used the published 3D reconstructions of the Golgi complex of Ladinsky *et al*. (1999) to estimate the probability of having round profiles in the vicinity of the cisternal rims of the Golgi, we found that in random sections, only 40% of round profiles visible within 40 nm of the cisternal rims represented cross sections of perforated domains of the Golgi cisternae (unpublished data). Assuming that the concentration of Golgi enzymes in perforated zones is on average 2.6-fold higher than that across the solid part of the cisternae (Table 2, miniwave, 0 min, GalT) and that these perforated zones give rise to 30% of the round profiles (see above) and the remaining 70% of the round profiles are 50- to 60-nm vesicles containing an ~10-fold lower concentration of Golgi enzymes (Table 2, miniwave, 0 min, GalT), the LD averaged over all near-rimmal round profiles would be equal to that over the cisternae (Figure 7E, miniwave, 0 min, GalTl).

The Role of Perforated Zones in Intra-Golgi Transport

What do these perforated zones represent? EM tomography clearly demonstrates that almost all Golgi cisternae have perforations near their rims and that the number of perforations does not depend on the position of a cisterna within the stack (Ladinsky *et al*., 1999). These perforations are thus found in all cisterna and often form clusters near the cisternal rims (Ladinsky *et al*., 1999; unpublished observations). To date, the role of these perforations and the mechanisms of their generation (or persistence) remain obscure, but some clues about their function may be found in recent in vitro studies. Based on the accumulation of Golgi enzymes in perforated zones of Golgi cisternae (this study), we consider it likely that these fusion-competent membranes enriched in Golgi enzymes derive from perforated zones.

Moreover, our data explain why the small fragments isolated by Lanoix *et al*. (1999) are enriched in ManII: they contain not only 50- to 60-nm vesicles but also high concentration of short cisternal fragments. Even before this, it was assumed that these small fragments were unlikely to be vesicles derived from COPI-coated buds, because their sizes ranged from 40 to 120 nm, in contrast to being extremely uniform. The size of these fragments is not typical of COPI-coated vesicles, which are very uniform in size and have an average diameter of ~52 nm (Marsh *et al*., 2001). Moreover, the light fraction isolated by Lanoix *et al*. (1999) was not capable of binding to and fusing with isolated Golgi membranes and thus of transferring Golgi enzymes (Love *et al*., 1998). Importantly, such membrane fragments enriched in Golgi enzymes are observed only after harsh treatments of cells, such as freeze-thawing, which induces the formation of ice crystals that damage membranes; Love *et al*., 1998) or high-salt washes of membranes (Lanoix *et al*., 1999, 2001). This harsh treatment can result in the breakdown of perforated zones enriched in Golgi enzymes into small membrane fragments (Balch *et al*., 1984). Finally, Pullikuth and Weidman (2002) showed that the release of *N*-acetylglucosamine transferase and GalT into the supernatant, which apparently contained small membrane fragments, occurred in a COPI-independent manner during an incubation of isolated Golgi membranes with cytosol. Therefore, we propose that these fusion-competent, low-density membrane fractions containing the transferases are formed from perforated areas of cisternae. The in vitro properties of these membrane fragments suggest that the membranes from which they derive are involved in enzyme transport between cisternae in vivo, but the underlying molecular mechanisms remain to be elucidated. Due to the extremely high purity of this light fraction, it seems to have a higher enzyme specific activity and concentration per unit of membrane surface than the original Golgi membranes, which would explain the data of Lanoix *et al*. (1999) regarding the relative concentration of Golgi enzymes in this fraction.

Possible Models of Intra-Golgi Transport

Thus, a cisternal maturation model that includes COPI-vesicle-mediated recycling of Golgi enzymes (reviewed in Elsner *et al*., 2003) does not fit our data. This model also implies that all of the cisternae should have COPI-coated buds for Golgi enzyme recycling. However, there are no COPI-coated buds on the last *trans*-cisternae (Ladinsky *et al*., 1999, 2002), whereas some Golgi enzymes, such as STF and fucosyltransferase, are present there (Rabouille *et al*., 1995). In this case, there is the possibility that Golgi-derived clathrin-coated vesicles serve for recycling of Golgi enzymes from the *trans*-most cisterna.

One plausible interpretation of our data is that Golgi enzymes recycle in polymorphic carriers that are generated by COP1-dependent fragmentation of the perforated zones, as COP1 can fragment cisternae to generate polymorphic elements enriched in Golgi enzymes (Lanoix *et al*., 1999; this study). The problem with this model is that no one (including ourselves, unpublished observations) has observed completely isolated or, at least, closed ended tubular intermediates containing high concentrations of Golgi enzymes in the Golgi area.

Among the possible models, one also can envisage a cisternal maturation/progression model based on retrograde diffusion of Golgi enzymes along connections between heterologous cisternae (the numbers of which increase after the arrival of cargo; Trucco *et al*., 2004). Alternatively, a carrier-maturation scheme (Mironov *et al*., 2001; Beznoussenko and Mironov, 2002) modified to include the formation of intercisternal connections after the arrival of cargo at the Golgi

(Trucco *et al*., 2004) also could serve as a working hypothesis of intra-Golgi transport. This implies that ER-derived transport carriers initially fuse with the *cis*-Golgi compartment. Then, the cargo domain fuses with the medial-Golgi, apparently triggering the physical separation of the cargo domain from the *cis*-Golgi. The subsequent fusion between the cargo-containing domain and the *trans*-Golgi compartment would induce separation of the cargo domain from the medial-Golgi. Thus, the same sequence of events (fusion, mixing, and resegregation) occur at each transfer step, with the intercisternal connections potentially serving for the fast diffusion of small soluble cargo through the Golgi.

ACKNOWLEDGMENTS

We thank Dr. C. P. Berrie for critical reading of the manuscript, Dr. J. Klumperman for critical evaluation of images, and who kindly provided cells, cDNAs, and antibodies. This study was funded by the Italian Association for Cancer Research (Milan, Italy); the Fondazione Telethon (Rome, Italy), grant number GP0203Y01; the Italian Ministero dell'Istruzione, dell'Università e della Ricerca (L.448/92-Project N.S209-P/F); the European Community (HPRN-CT-2002-00259, to A.L. and K.N.J.B.); the Royal Netherlands Academy of Arts and Sciences (to A.J.K); and FEI Company (to W.J.C.G. and K.N.J.B).

REFERENCES

Balch, W.E., Glick, B.S., and Rothman, J.E. (1984). Sequential intermediates in the pathway of intercompartmental transport in a cell-free system. Cell. *39*, 525–536.

Band, A.M., Maatta, J., Kaariainen, L., and Kuismanen, E. (2001). Inhibition of the membrane fusion machinery prevents exit from the TGN and proteolytic processing by furin. FEBS Lett. *505*, 118–124.

Barnard, R.J., Morgan, A., and Burgoyne, R.D. (1996). Domains of alpha-SNAP required for the stimulation of exocytosis and for N-ethylmalemide-sensitive fusion protein (NSF) binding and activation. Mol. Biol. Cell. *7*, 693–701.

Beznoussenko, G.V., and Mironov, A.A. (2002). Models of intracellular transport and evolution of the Golgi complex. Anat. Rec. *268*, 226–238.

Bonfanti, L., Mironov, A.A., Jr., Martinez-Menarguez, J.A., Martella, O., Fusella, A., Baldassarre, M., Buccione, R., Geuze, H.J., Mironov, A.A., and Luini, A. (1998). Procollagen traverses the Golgi stack without leaving the lumen of cisternae: evidence for cisternal maturation. Cell. *95*, 993–1003.

Brown, W.J., and Farquhar, M.G. (1989). Immunoperoxidase methods for the localization of antigens in cultured cells and tissue sections by electron microscopy. Methods Cell Biol. *31*, 553–569.

Cosson, P., Amherdt, M., Rothman, J.E., and Orci, L. (2002). A resident Golgi protein is excluded from peri-Golgi vesicles in NRK cells. Proc. Natl. Acad. Sci. USA *99*, 12831–12834.

Dominguez, M., Dejgaard, K., Fullekrug, J., Dahan, S., Fazel, A., Paccaud, J.P., Thomas, D.Y., Bergeron, J.J., and Nilsson, T. (1998). gp25L/emp24/p24 protein family members of the cis-Golgi network bind both COP I and II coatomer. J. Cell Biol. *140*, 751–765.

Elsner, M., Hashimoto, H., and T. Nilsson. (2003). Cisternal maturation and vesicle transport: join the band wagon! Mol. Membr. Biol. *20*, 221–229.

Godi, A., *et al*. (1998). ADP ribosylation factor regulates spectrin binding to the Golgi complex. Proc. Natl. Acad. Sci. USA *95*, 8607–8612.

Griffiths, G. (2000). Gut thoughts on the Golgi complex. Traffic. *1*, 738–745.

Jokitalo, E., Cabrera-Poch, N., Warren, G., and Shima, D.T. (2001). Golgi clusters and vesicles mediate mitotic inheritance independently of the endoplasmic reticulum. J. Cell Biol. *154*, 317–330.

Ladinsky, M.S., Mastronarde, D.N., McIntosh, J.R., Howell, K.E., and Staehelin, L.A. (1999). Golgi structure in three dimensions: functional insights from the normal rat kidney cell. J. Cell Biol. *144*, 1135–1149.

Ladinsky M.S., Wu CC, McIntosh S, McIntosh JR, and Howell KE. 2002. Structure of the Golgi and distribution of reporter molecules at 20 degrees C reveals the complexity of the exit compartments. Mol. Biol. Cell *13*, 2810–2825.

Lanoix, J., Ouwendijk, J., Lin, C.C., Stark, A., Love, H.D., Ostermann, J., and Nilsson, T. (1999). GTP hydrolysis by arf-1 mediates sorting and concentration of Golgi resident enzymes into functional COP I vesicles. EMBO J. *18*, 4935–4948.

Lanoix, J., Ouwendijk, J., Stark, A., Szafer, E., Cassel, D., Dejgaard, K., Weiss, M., and Nilsson, T. (2001). Sorting of Golgi resident proteins into different subpopulations of COPI vesicles: a role for ArfGAP1. J. Cell Biol. *155*, 1199–1212.

Love, H.D., Lin, C.C., Short, C.S., and Ostermann, J. (1998). Isolation of functional Golgi-derived vesicles with a possible role in retrograde transport. J. Cell Biol. *140*, 541–551.

Marsh, B.J., Mastronarde, D.N., McIntosh, J.R., and Howell, K.E. (2001). Structural evidence for multiple transport mechanisms through the Golgi in the pancreatic beta-cell line, HIT-T15. Biochem. Soc. Trans. *29*, 461–467.

Martinez-Menarguez, J.A., Prekeris, R., Oorschot, V.M., Scheller, R., Slot, J.W., Geuze, H.J., and Klumperman, J. (2001). Peri-Golgi vesicles contain retrograde but not anterograde proteins consistent with the cisternal progression model of intra-Golgi transport. J. Cell Biol. *155*, 1213–1224.

Mayhew, T., Griffiths, G., Habermann, A., Lucocq, J., Emre, N., and Webster, P. (2003). A simpler way of comparing the labelling densities of cellular compartments illustrated using data from VPARP and LAMP-1 immunogold labelling experiments. Histochem. Cell Biol. *119*, 333–341.

Mironov, A.A., *et al*. (2001). Small cargo proteins and large aggregates can traverse the Golgi by a common mechanism without leaving the lumen of cisternae. J. Cell Biol. *155*, 1225–1238.

Misteli, T., and Warren, G. (1994). COP-coated vesicles are involved in the mitotic fragmentation of Golgi stacks in a cell-free system. J. Cell Biol. *125*, 269–282.

Misteli, T., and Warren, G. (1995). Mitotic disassembly of the Golgi apparatus in vivo. J. Cell Sci. *108*, 2715–2727.

Morre, D.J., and Keenan, T.W. (1994). Golgi apparatus buds - vesicles or coated ends of tubules? Protoplasma *179*, 1–4.

Orci, L., Amherdt, M., Ravazzola, M., Perrelet, A., and Rothman, J.E. (2000). Exclusion of Golgi residents from transport vesicles budding from Golgi cisternae in intact cells. J. Cell Biol. *150*, 1263–1270.

Orci, L., Stamnes, M., Ravazzola, M., Amherdt, M., Perrelet, A., Sollner, T.H., and Rothman, J.E. (1997). Bidirectional transport by distinct populations of COPI-coated vesicles. Cell *90*, 335–349.

Pepperkok, R., Scheel, J., Horstmann, H., Hauri, H.P., Griffiths, G., and Kreis, T.E. (1993). Beta-COP is essential for biosynthetic membrane transport from the endoplasmic reticulum to the Golgi complex in vivo. Cell *74*, 71–82.

Polishchuk, R.S., Polishchuk, E.V., Marra, P., Alberti, S., Buccione, R., Luini, A., and Mironov, A.A. (2000). Correlative light-electron microscopy reveals the tubular-saccular ultrastructure of carriers operating between Golgi apparatus and plasma membrane. J. Cell Biol. *148*, 45–58.

Pullikuth, A.K., and Weidman, P.J. (2002). In vitro transport on cis and trans sides of the Golgi involves two distinct types of coatomer and ADP-ribosylation factor-independent transport intermediates. J. Biol. Chem. *277*, 50355–50364.

Rabouille, C., Hui, N., Hunte, F., Kieckbusch, R., Berger, E.G., Warren, G., and Nilsson, T. (1995). Mapping the distribution of Golgi enzymes involved in the construction of complex oligosaccharides. J. Cell Sci. *108*, 1617–1627.

Rojo, M., Pepperkok, R., Emery, G., Kellner, R., Stang, E., Parton, R.G., and Gruenberg, J. (1997). Involvement of the transmembrane protein p23 in biosynthetic protein transport. J. Cell Biol. *139*, 1119–1135.

Stinchcombe, J.C., Nomoto, H., Cutler, D.F., and Hopkins, C.R. (1995). Anterograde and retrograde traffic between the rough endoplasmic reticulum and the Golgi complex. J. Cell Biol. *131*, 1387–1401.

Velasco, A., Hendricks, L., Moremen, K.W., Tulsiani, D.R., Touster, O., and Farquhar, M.G. (1993). Cell type-dependent variations in the subcellular distribution of alpha-mannosidase I and II. J. Cell Biol. *122*, 39–51.

Weidman, P., Roth, R., and Heuser, J. (1993). Golgi membrane dynamics imaged by freeze-etch electron microscopy: views of different membrane coatings involved in tubulation versus vesiculation. Cell. *75*, 123–133.

Yang, J.S., Lee, S.Y., Gao, M., Bourgoin, S., Randazzo, P.A., Premont, R.T., and Hsu, V.W. (2002). ARFGAP1 promotes the formation of COPI vesicles, suggesting function as a component of the coat. J. Cell Biol. *159*, 69–78.